

Green's Functions and Boundary Integral Analysis for Exponentially Graded Materials: Heat Conduction

L. J. Gray¹ T. Kaplan¹ J. D. Richardson¹

Glaucio H. Paulino²

November 27, 2000

¹Computer Science and Mathematics Division, Oak Ridge National Laboratory,
Oak Ridge, Tennessee 37831-6367 *ljg@ornl.gov*

²Department of Civil and Environmental Engineering, University of Illinois at
Urbana-Champaign, Urbana, IL 61801-2352 *paulino@uiuc.edu*

Abstract

Free space Green's functions are derived for graded materials in which the thermal conductivity varies exponentially in one coordinate. Closed form expressions are obtained for the steady state diffusion equation, in two and three dimensions. The corresponding boundary integral equation formulations for these problems are derived, and the three-dimensional case is solved numerically using a Galerkin approximation. The results of test calculations are in excellent agreement with exact solutions and finite element simulations.

Key words. Green's functions, functionally graded materials, diffusion, boundary integral analysis, Galerkin approximation.

Abbreviated title: Green's functions for FGMs

1 Introduction

Functionally graded materials (FGMs) are an important area of materials science research, with potentially many important applications, e.g., super-heat resistance materials for thermal barrier coatings and furnace liners, vehicle and personal body armor, electromagnetic sensors, and graded refractive index materials for optical applications. In an ideal FGM, the material properties may vary smoothly in one dimension (e.g., are constant in (x, y) but vary with z). As an example, having a smooth transition region between a pure metal and pure ceramic would result in a material that combines the desirable high temperature properties and thermal resistance of a ceramic, with the fracture toughness of a metal. Comprehensive reviews of current FGM research may be found in the articles by Hirai [9] and Markworth *et al.* [15], and the book by Suresh and Mortensen [23].

Computational analysis can be an effective method for designing specific FGM systems, and for understanding FGM behavior. For homogeneous media, boundary integral equation methods [3] have been used extensively. However, the reformulation in terms of integral equations relies upon having, as either a closed form or a computable expression, a fundamental solution (Green's function) of the partial differential equation. Application of the boundary integral technique has therefore been limited, almost exclusively, to homogeneous, or piece-wise homogeneous, media.

The fundamental solutions traditionally employed in boundary integral analysis for homogeneous materials are 'free space' Green's functions: they satisfy the appropriate differential equation everywhere in space, except at the site where a point load driving force is applied. Derivations for some of the basic Green's functions can be found in [2, 3]. There has also been work in the direction of deriving Green's functions for a general non-homogeneous material [1, 6, 18, 19, 20]. Steady state heat conduction with an arbitrary spatially varying conductivity has recently been investigated [7, 10] and has generated some debate in the literature [4, 17]. In most cases, exact Green's functions are only obtained under certain restrictions.

Relatively little attention has been paid to obtaining Green's functions for the special case of graded materials: a Green's function for a special type of

elastodynamics problem was obtained by Vrettos [24]. In the present paper, we derive free space fundamental solutions for both the two-dimensional (2D) and three-dimensional (3D) FGM Laplace equation, assuming that the thermal conductivity varies exponentially. The corresponding boundary integral equation formulation, which turns out to be somewhat different from the homogeneous media case, is also obtained. The 2D results have appeared in conjunction with a convective heat transfer problem in a *homogeneous* material [13, 25]. It is expected that the derivation of the three-dimensional Green's function will carry over to other FGM applications, and thus this analysis is presented in detail.

This paper is organized as follows. The 3D Laplace equation is treated in Section 2.1, and the 2D case in Section 2.2. Section 3 discusses some test results from a Galerkin numerical implementation of the boundary integral formulation, and Section 4 contains some concluding remarks. Finally, in Appendix A it is shown that the integral equations and Green's functions can be suitably modified to allow for a Symmetric-Galerkin implementation. For $k(z)$ real, and for the re-formulated equations, complete formulas for the fundamental solutions and their first and second derivatives are given in this appendix.

2 Green's Functions

Steady state isotropic heat conduction in a solid is governed by the equation

$$\nabla \cdot (k \nabla \phi) = 0 . \quad (1)$$

Here $\phi = \phi(x, y, z)$ is the temperature function, and we assume the functionally graded material is defined by the thermal conductivity

$$k(x, y, z) = k(z) = k_0 e^{-2i\alpha z} , \quad (2)$$

where α is real. This assumption of a purely imaginary exponent is apparently necessary for the derivation that follows. However, once the solution is obtained, it is readily seen to be valid for any complex α . Substituting Eq. (2) into Eq. (1), one obtains that the temperature satisfies

$$\nabla^2 \phi - 2i\alpha \phi_z = 0 , \quad (3)$$

where ϕ_z denotes the derivative with respect to z .

The Green's function equation can be derived by constructing the integral equation corresponding to Eq. (3). Following the standard procedure, Eq. (3) is multiplied by an arbitrary function $f(x, y, z) = f(Q)$ and integrated over a bounded volume V . Integrating by parts, and denoting the boundary of V by Σ , one obtains

$$\begin{aligned} 0 &= \int_V f(Q) \left(\nabla^2 \phi(Q) - 2i\alpha \phi_z(Q) \right) dV_Q \\ &= \int_\Sigma \left\{ f(Q) \frac{\partial}{\partial n} \phi(Q) - \phi(Q) \frac{\partial}{\partial n} f(Q) - 2i\alpha n_z(Q) \phi(Q) f(Q) \right\} dQ \\ &\quad + \int_V \phi(Q) \left(\nabla^2 f(Q) + 2i\alpha f_z(Q) \right) dV_Q, \end{aligned} \quad (4)$$

where $n(Q) = (n_x, n_y, n_z)$ is the unit outward normal for Σ . If $f(Q) = G(P, Q)$ satisfies the Green's function equation (the adjoint to Eq. (3))

$$\nabla^2 G(P, Q) + 2i\alpha G_z(P, Q) = -\delta(Q - P), \quad (5)$$

where δ is the Dirac delta function, and the remaining volume integral becomes simply $-\phi(P)$. Thus we obtain the governing boundary integral equation

$$\begin{aligned} \phi(P) + \int_\Sigma \phi(Q) \left(\frac{\partial}{\partial n} G(P, Q) + 2i\alpha n_z G(P, Q) \right) dQ = \\ \int_\Sigma G(P, Q) \frac{\partial}{\partial n} \phi(Q) dQ, \end{aligned} \quad (6)$$

which differs in form from the usual integral statements by the presence of the additional term multiplying $\phi(Q)$. With obvious changes (e.g., line integrals instead of surface integrals), the above equations are equally valid for two dimensions. We first derive the Green's function for three dimensions.

2.1 Three Dimensions

Let $\hat{f}(\boldsymbol{\omega})$ denote the Fourier transform of a function $\mathcal{F}(Q)$,

$$\hat{f}(\boldsymbol{\omega}) = \int_{\mathcal{R}^3} f(Q) e^{-i\boldsymbol{\omega} \cdot \mathbf{Q}} dQ \quad (7)$$

where $\boldsymbol{\omega} = (\omega_x, \omega_y, \omega_z)$ is the transform variable and the dot represents inner product. Transforming Eq. (5) and solving for $\hat{G}(\boldsymbol{\omega})$ (the transform of G with respect to Q), yields

$$\hat{G}(\boldsymbol{\omega}) = \frac{e^{-i\boldsymbol{\omega}\cdot P}}{\omega^2 + 2\alpha\omega_z}, \quad (8)$$

where $\omega^2 = \boldsymbol{\omega}\cdot\boldsymbol{\omega}$. Applying the inverse transform, one obtains

$$G(P, Q) = \frac{1}{(2\pi)^3} \int_{\mathcal{R}^3} \frac{e^{i\boldsymbol{\omega}\cdot(Q-P)}}{\omega^2 + 2\alpha\omega_z} d\boldsymbol{\omega}, \quad (9)$$

where $d\boldsymbol{\omega}$ is shorthand for the three-dimensional differential element, i.e. $d\boldsymbol{\omega} = d\omega_x d\omega_y d\omega_z$. Changing variables

$$\omega_z \rightarrow \omega_z - \alpha \quad (10)$$

and setting $R = Q - P$, $R_z = Q_z - P_z$, we obtain

$$G(P, Q) = \frac{1}{(2\pi)^3} e^{-i\alpha R_z} \int_{\mathcal{R}^3} \frac{e^{i\boldsymbol{\omega}\cdot R}}{\omega^2 - \alpha^2} d\boldsymbol{\omega}, \quad (11)$$

which can be conveniently split into two terms,

$$G(P, Q) = \frac{e^{-i\alpha R_z}}{(2\pi)^3} \left[\int_{\mathcal{R}^3} \frac{e^{i\boldsymbol{\omega}\cdot R}}{\omega^2} d\boldsymbol{\omega} + \alpha^2 \int_{\mathcal{R}^3} \frac{e^{i\boldsymbol{\omega}\cdot R}}{\omega^2 (\omega^2 - \alpha^2)} d\boldsymbol{\omega} \right]. \quad (12)$$

The first integral is Eq. (9) with $\alpha = 0$, and is therefore recognized as the Green's function for the Laplace equation (constant k), the point source potential:

$$\frac{e^{-i\alpha R_z}}{(2\pi)^3} \int_{\mathcal{R}^3} \frac{e^{i\boldsymbol{\omega}\cdot R}}{\omega^2} d\boldsymbol{\omega} = \frac{e^{-i\alpha R_z}}{4\pi r}, \quad (13)$$

where $r = \|R\| = \|Q - P\|$ is the distance between the source point P and the field point Q .

To evaluate the second term in Eq. (12), it is convenient to employ spherical coordinates (ρ, θ, ψ) , with however, the axis defining the pole $\psi = 0$ taken as the direction R/r instead of the z -axis (see Figure 1), and $-\infty < \rho < \infty$,

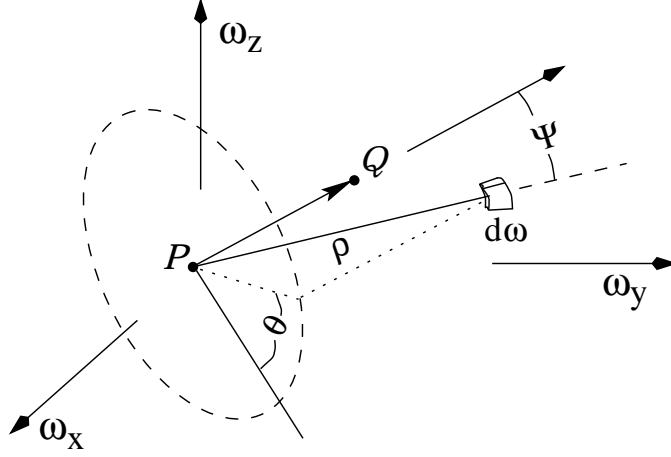


Figure 1: Spherical coordinate system for evaluating the ω integral.

$0 \leq \psi \leq \pi/2$, and $0 \leq \theta \leq 2\pi$. Noting that $\omega \cdot R = \rho r \cos(\psi)$ and that the integrand is independent of θ , this second term therefore becomes

$$\frac{\alpha^2 e^{-i\alpha R_z}}{(2\pi)^2} \int_0^{\pi/2} \sin(\psi) d\psi \int_{-\infty}^{\infty} \frac{e^{i\rho r \cos(\psi)}}{\rho^2 - \alpha^2} d\rho. \quad (14)$$

Using the contour shown in Figure 2, the ρ integration is a straightforward exercise in residue calculus, yielding

$$\int_{-\infty}^{\infty} \frac{e^{i\rho r \cos(\psi)}}{\rho^2 - \alpha^2} d\rho = -\frac{\pi}{\alpha} \sin(\alpha r \cos(\psi)). \quad (15)$$

The final integration,

$$-\frac{\pi}{\alpha} \int_0^{\pi/2} \sin(\psi) \sin(\alpha r \cos(\psi)) d\psi \quad (16)$$

follows from a simple change of variables, and thus the second term is seen to be

$$\frac{e^{-i\alpha R_z} \cos(\alpha r)}{4\pi r} - \frac{e^{-i\alpha R_z}}{4\pi r}. \quad (17)$$

Including Eq. (13), we find the simple result

$$G(P, Q) = \frac{e^{-i\alpha R_z} \cos(\alpha r)}{4\pi r}. \quad (18)$$

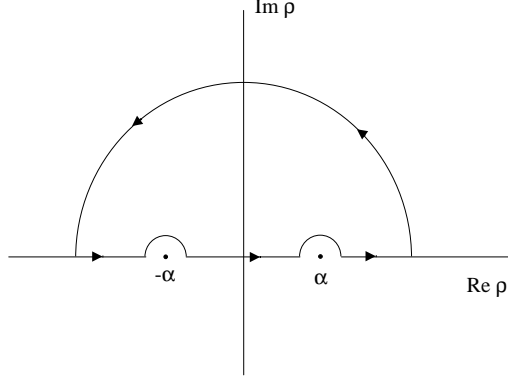


Figure 2: Contour in the complex plane used to compute the ρ integration.

Although this result was derived assuming that α is real, it is a simple matter to check by direct calculation that Eq. (18) satisfies Eq. (5) for any complex α . It is useful, especially for the discussion of the 2D case that follows, to observe that

$$G(P, Q) = e^{-i\alpha R_z} \frac{e^{-i\alpha r}}{4\pi r} \quad (19)$$

is an equally valid solution of Eq. (5) for α real. Moreover, the added $\sin(\alpha r)/r$ term is regular as $r \rightarrow 0$, and thus does not alter the delta function at $Q = P$. Replacing α by $i\beta_0$, where β_0 is real, we obtain

$$G(P, Q) = \frac{e^{\beta_0(r+R_z)}}{4\pi r} \quad (20)$$

as the Green's function for $k(z) = e^{2\beta_0 z}$.

In the derivation of the boundary integral equation, a sphere S_ε of radius ε centered at the interior point P would be removed from V , and the integration over Σ would include the surface of this sphere. The limit as $\varepsilon \rightarrow 0$ of the integral

$$\int_{S_\varepsilon} \left\{ G(P, Q) \frac{\partial}{\partial n} \phi(Q) - \phi(Q) \frac{\partial}{\partial n} G(P, Q) - 2i\alpha (\phi(Q) G(P, Q)) n_z \right\} dQ \quad (21)$$

must therefore be considered. However, for $r \rightarrow 0$,

$$\frac{\partial}{\partial n} G(P, Q) \approx \frac{\partial}{\partial n} \frac{1}{4\pi r} \quad (22)$$

and the $\varepsilon = 0$ limit does indeed produce the correct value $-\phi(P)$.

Finally, it is useful to note that Eq. (17) can, from the point of view of the singularity at $r = 0$, be considered as a remainder term. That is, the singularity for the FGM Green's function is entirely contained within Eq. (13), the homogeneous steady state solution, as Eq. (17) is regular at $r = 0$.

2.2 Two Dimensions

The Green's function $g(x_Q, z_Q; x_P, z_P)$ for the 2D equation,

$$\phi_{xx} + \phi_{zz} - 2i\alpha\phi_z = 0, \quad (23)$$

is expected to behave as $\log(r)$, and as this function does not die off at infinity, the above Fourier transform approach is doomed to fail. However, this fundamental solution can be viewed as the response seen at the point $(x_Q, 0, z_Q)$ to a uniform distribution of charge along the y -axis. This response should be the result of integrating the three-dimensional Green's function over this axis, which for the homogeneous case takes the form

$$\frac{1}{4\pi} \int_{-\infty}^{\infty} \frac{dy_P}{((x_Q - x_P)^2 + y_P^2 + (z_Q - z_P)^2)^{1/2}}. \quad (24)$$

The fact that the integral doesn't exist is a minor inconvenience that is remedied by doing the analysis for $\partial G / \partial x_Q$ [11]. The integral of this function with respect to y_P does exist, and followed by an integration over x_Q , the correct $\log(r)$ result is obtained, where r is now the 2D distance.

With this framework in mind, we observe that the three-dimensional FGM Green's function, in the form of Eq. (19), is $e^{-i\alpha R_z}$ times the fundamental solution for the Helmholtz equation [3]. Since this prefactor is independent of y_P , integrating out this coordinate as in Eq. (24), we expect that the 2D FGM Green's function is given by

$$g(x_Q, z_Q; x_P, z_P) = \frac{i}{4} e^{-i\alpha R_z} H_0^1(\alpha r). \quad (25)$$

Here, H_0^1 is the zeroth order first kind Hankel function [16], well known to be the solution of the Helmholtz equation in two dimensions. This expectation can be established simply by differentiating Eq. (25) and checking that

$$g_{xx} + g_{zz} + 2i\alpha g_z = 0 , \quad (26)$$

for $Q \neq P$ (this is the 2D analogue of the Green's function equation, Eq. (5)). A simple symbolic computation program which performs the verification can be found in Appendix B. That this differentiation also yields a delta function at $Q = P$ follows from the known behavior of H_0^1 for the Helmholtz equation. Finally, it should be noted that the 2D boundary integral equation becomes

$$\begin{aligned} \phi(P) + \int_{\Sigma} \phi(Q) \left(\frac{\partial}{\partial n} g(P, Q) + 2i\alpha n_z g(P, Q) \right) dQ = \\ \int_{\Sigma} g(P, Q) \frac{\partial}{\partial n} \phi(Q) dQ , \end{aligned} \quad (27)$$

which corresponds to Eq. (6) with $G(P, Q)$ (3D case) replaced by $g(P, Q)$ (2D case).

2.3 Extensions

As it may be useful to have the material properties vary in more than one component [12], it is worth noting that the above analysis extends to a more general exponential variation for \mathbf{k} ,

$$\mathbf{k}(x, y, z) = k_0 e^{-2i\boldsymbol{\alpha} \cdot \mathbf{Q}} , \quad (28)$$

where $\boldsymbol{\alpha} = (\alpha_x, \alpha_y, \alpha_z)$. The three-dimensional Green's function is now given by

$$G_{xyz}(P, Q) = \frac{e^{-i\boldsymbol{\alpha} \cdot \mathbf{R}} \cos((\boldsymbol{\alpha} \cdot \boldsymbol{\alpha})r)}{4\pi r} . \quad (29)$$

Comparing this with Eq. (18), it is not surprising that the 2D result in this case (again dropping out the y coordinate) becomes

$$g_{xz}(x_Q, z_Q; x_P, z_P) = \frac{i}{4} e^{-i\boldsymbol{\alpha} \cdot \mathbf{R}} H_0^1((\boldsymbol{\alpha} \cdot \boldsymbol{\alpha})r) . \quad (30)$$

2.4 Galerkin approximation

The numerical results presented in the next section utilize the Galerkin approximation [3] to reduce the integral equation to a finite system of equations. Here we briefly review this technique, starting by rewriting Eq. (6) as

$$\begin{aligned} \mathcal{P}(P) \equiv \phi(P) + \int_{\Sigma} \phi(Q) \left(\frac{\partial}{\partial n} G(P, Q) + 2i\alpha n_z G(P, Q) \right) dQ - \\ \int_{\Sigma} G(P, Q) \frac{\partial}{\partial n} \phi(Q) dQ = 0 \end{aligned} \quad (31)$$

As is usual, basis shape functions $\psi_j(Q)$ are used to interpolate the boundary from the element nodal coordinates, and to approximate the surface potential and flux in terms of nodal values, *i.e.*,

$$\begin{aligned} \Sigma(\eta, \xi) &= \sum_j (x_j, y_j, z_j) \psi_j(\eta, \xi) \\ \phi(Q) &= \sum_j \phi_j \psi_j(Q) \\ \frac{\partial \phi}{\partial n}(Q) &= \sum_j \left(\frac{\partial \phi}{\partial n} \right)_j \psi_j(Q) \end{aligned} \quad (32)$$

The numerical results reported herein employ a six-noded quadratic triangular element, defined using the right triangle parameter space (η, ξ) , $\eta \geq 0$, $\xi \geq 0$, $\eta + \xi \leq 1$. The shape functions are given by

$$\begin{aligned} \psi_1(\eta, \xi) = (1 - \eta - \xi)(1 - 2\eta - 2\xi) & \quad \psi_4(\eta, \xi) = 4\eta(1 - \eta - \xi) \\ \psi_2(\eta, \xi) = \eta(2\eta - 1) & \quad \psi_5(\eta, \xi) = 4\eta\xi \\ \psi_3(\eta, \xi) = \xi(2\xi - 1) & \quad \psi_6(\eta, \xi) = 4\xi(1 - \eta - \xi) \end{aligned} \quad (33)$$

In a Galerkin approximation, these shape functions are employed as weighting functions for enforcing Eq. (31) ‘on average’, *i.e.*,

$$\int_{\Sigma} \psi_k(P) \int_{\Sigma} \mathcal{P}(P) dP = 0 . \quad (34)$$

When the approximations in Eq. (32) are incorporated into this equation, the resulting finite system of equations can be discretized and solved numerically.

It should also be noted that, unlike the Green's function $1/(4\pi r)$ for the Laplace equation (homogeneous problem), neither Eq. (19) nor Eq. (25) is a symmetric function of P and Q . It would therefore appear impossible to have a symmetric-Galerkin approximation [5, 8, 14, 21, 22], as this formulation demands a symmetric Green's function. However, as shown in the appendix, a slight reworking of the equations and the kernel functions restores all of the necessary symmetry properties. This appendix also provides formulas for all of the kernel functions: temperature and flux equations in two and three dimensions.

3 Numerical Examples

The three-dimensional steady state fundamental solution has been incorporated into a boundary element method (BEM) algorithm. As noted above, the integral equation (6) is numerically approximated via the (non-symmetric) Galerkin method (see Eq. (34)), together with standard six-node isoparametric quadratic triangular elements to interpolate the boundary and boundary functions. For the numerical examples, the conservation equation (1) will be taken as energy conservation in a functionally graded media under the condition of steady state heat conduction without volumetric generation.

3.1 Unit Cube: Constant ϕ on Two Planes

For the first example problem, the geometry is a unit cube with the origin of a Cartesian system fixed at one corner. The thermal conductivity in this example is taken to be

$$k(z) = k_0 e^{2\beta z} = 5e^{3z}. \quad (35)$$

The top face of the cube [$z = 1$] is maintained at a temperature of $T_1 = 100^\circ$ while the bottom face [$z = 0$] is maintained at $T_0 = 0^\circ$. The remaining four faces are insulated (zero normal flux).

With these imposed boundary conditions, the problem is one-dimensional

in nature (independent of x and y) and has a simple exact solution. The temperature field and heat flux vectors are given by

$$\begin{aligned}\phi &= T_1 \frac{1 - e^{-2\beta z}}{1 - e^{-2\beta}} \\ \mathbf{q} &= -k_o T_1 \frac{2\beta}{1 - e^{-2\beta}} \hat{\mathbf{k}}\end{aligned}\tag{36}$$

where $\hat{\mathbf{k}}$ is a unit vector in the z -direction.

Numerical solutions for the temperature profile for this problem are shown in Figure 3. The plot also includes the results obtained from a finite element method (FEM) simulation using a commercial package. In the FEM simulation, forty homogeneous layers were used to approximate the continuous grading; the conductivity of each layer was computed from Eq. (35) where z was taken as the z -coordinate of the layer's centroid. The FEM elements used were 20-node quadratic brick elements and each of the forty layers contained 400 brick elements, resulting in a total of 69,720 nodes. In the BEM solution, a uniform grid consisting of isosceles right triangles, with each leg having length 0.1, was employed, resulting in a total of 1200 elements and 2,646 nodes.

3.2 Unit Cube: Linear Heat Flux

The second problem once again employs the unit cube previously described with the thermal conductivity again given by Eq. (35). However, the cube is now insulated on the faces $[y = 0]$ and $[y = 1]$, while uniform heat fluxes of $5000 \left[\frac{\text{POWER}}{\text{AREA}} \right]$ are added and removed, respectively, at the $[x = 1]$ and $[x = 0]$ faces. In addition, the $[z = 0]$ face is specified to have an x -dependent temperature distribution $T = 1000 x^\circ$ and at $[z = 1]$ a normal heat flux of $q = 15000 x$ is removed. The analytic solution for this problem is

$$\begin{aligned}T &= 1000 x e^{-3z} \\ \mathbf{q} &= -5000 \hat{\mathbf{i}} + 15000 x \hat{\mathbf{k}}\end{aligned}\tag{37}$$

where $\hat{\mathbf{i}}$ is a unit vector in the x -direction.

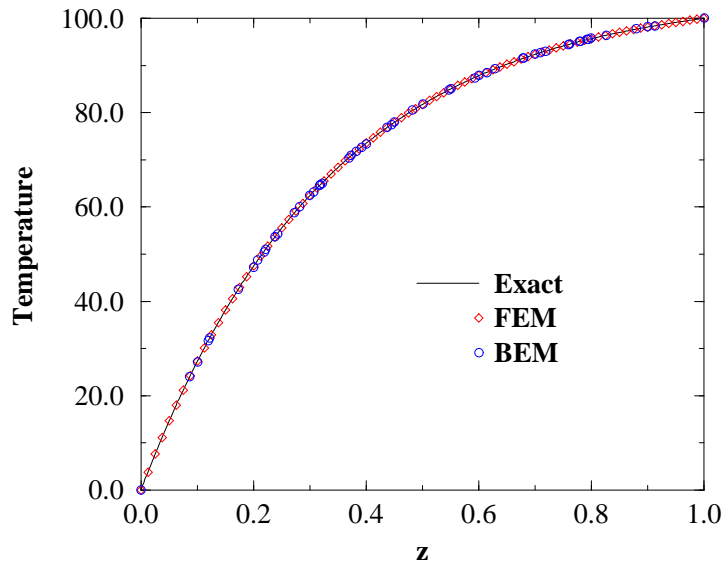


Figure 3: Temperature distribution in the FGM unit cube.

The results of the numerical simulations for the temperature distributions along an edge are shown in Figure 4. The FEM and BEM discretizations for this problem are identical to those used in the previous example.

3.3 FGM Rotor

The final numerical example will be a rotor with eight mounting holes. Due to the anticipated axisymmetric nature of the problem only one-eighth of the rotor will be modeled as drawn in Figure 5. The grading direction for the

rotor is parallel to its line of axisymmetry which will be taken as the z -axis. The thermal conductivity for the rotor will vary according to

$$k(z) = 20e^{330z} \frac{\text{W}}{\text{m} \cdot ^\circ\text{K}}. \quad (38)$$

A schematic for the thermal boundary conditions is shown in Figure 6. The temperature is specified along the inner and outer radii and a uniform heat flux of $5 \times 10^5 \text{ W/m}^2$ is added on the bottom surface where $z = 0$. All other surfaces are insulated as shown.

The BEM solution will be compared with an FEM solution obtained from the same package used in the previous examples using ten-node tetrahedral elements to handle the geometric complexity of the rotor. Due to resource limitations, the FEM model was limited to 12 layers which resulted in the rather crude conductivity profile shown in Figure 7. Even so, the FEM mesh required 95,880 nodes, whereas the BEM mesh employed 3,252. The mesh employed for the boundary integral analysis is shown in Figure 8.

The temperature distribution around the hole is shown in Figure 9. The angle θ is measured from a line passing through the line of axisymmetry for the problem and the center line of the hole as shown in Figure 9. Though the surface nodal positions in the two models were not coincident in general, the plot shows a strong agreement in the two solutions.

The radial heat flux along the line shown as the interior corner in Figure 6 is plotted in Figure 10. The negative sign indicates that the flow of heat is toward the interior of the rotor. A limitation on the use of piece-wise constant conductivities in FEM models may be evident in the plot where the FEM nodal value at $z = 0.01$ seems to fall out of line with the other values on the curve. The behavior should be fully expected, however, given the local error associated with the piece-wise constant approximation seen near $z = 0.01$ in Figure 7. As should also be expected, the nodal flux values from the BEM solution seem to fall onto a single curve even in the region of the steepest conductivity gradient.

4 Conclusions

The primary conclusion of this work is that boundary integral analysis, for the most part limited to applications involving homogeneous or piece-wise homogeneous media, can be successfully applied to exponentially graded materials. Although the simplest case, namely the Laplace equation, has been treated herein, it is expected that other applications, most notably transient diffusion and elasticity, can also be addressed. These topics are currently being investigated. Note that a specific elastodynamics problem has already been addressed by Vrettos [24].

The numerical results presented in this paper have shown that it is simple to implement the FGM Green's function in a standard boundary integral (Galerkin) approximation, and that accurate results are obtained. For graded materials, this offers the possibility of efficient and accurate solution of those types of problems for which a boundary integral analysis is particularly advantageous, such as shape optimization, moving boundaries, and small scale structures.

Acknowledgments

This research was supported in part by the Applied Mathematical Sciences Research Program of the Office of Mathematical, Information, and Computational Sciences, U.S. Department of Energy under contract DE-AC05-00OR22725 with UT-Battelle, LLC. Additional support was provided by the Laboratory Directed Research and Development Program of the Oak Ridge National Laboratory. G. H. Paulino acknowledges the support from the National Science Foundation under grant CMS-9996378 (Mechanics and Materials Program). The authors would like to thank Profs. J. Berger and P. A. Martin for useful discussions, and Prof. Luiz Wrobel for pointing out the paper by Li and Evans.

References

- [1] W. T. ANG, J. KUSUMA, AND D. L. CLEMENTS, *A boundary element method for a second order elliptic partial differential equation with variable coefficients*, *Engrg. Analy. Boundary Elements*, 18 (1996), pp. 311–316.
- [2] G. BARTON, *Elements of Green's Functions and Propagation*, Oxford University Press, Oxford, 1999.
- [3] M. BONNET, *Boundary Integral Equation Methods for Solids and Fluids*, Wiley and Sons, England, 1995.
- [4] M. BONNET AND M. GUIGGIANI, *Comments about the paper entitled 'a generalized boundary integral equation for isotropic heat conduction with spatially varying thermal conductivity' by A. J. Kassab and E. Divo*, *Engrg. Analy. Boundary Elements*, 22 (1998), pp. 235–240.
- [5] M. BONNET, G. MAIER, AND C. POLIZZOTTO, *Symmetric Galerkin boundary element method*, *ASME Appl. Mech. Rev.*, 51 (1998), pp. 669–704.
- [6] D. L. CLEMENTS, *A boundary integral equation method for the numerical solution of a second order elliptic equation with variable coefficients*, *J. Austral. Math. Soc. (Series B)*, 22 (1980), pp. 218–228.
- [7] E. DIVO AND A. J. KASSAB, *Generalized boundary integral equation for heat conduction in non-homogeneous media: recent developments on the sifting property*, *Engrg. Analy. Boundary Elements*, 22 (1998), pp. 221–234.
- [8] F. HARTMANN, C. KATZ, AND B. PROTOPSALTIS, *Boundary elements and symmetry*, *Ingenieur-Archiv*, 55 (1985), pp. 440–449.
- [9] T. HIRAI, *Functionally graded materials*, vol. 17B of *Processing of Ceramics*, Part 2, VCH Verlagsgesellschaft mbH, Weinheim, Germany, 1996, pp. 292–341.

- [10] A. J. KASSAB AND E. DIVO, *A generalized boundary integral equation for isotropic heat conduction with spatially varying thermal conductivity*, *Engrg. Analy. Boundary Elements*, 18 (1996), pp. 273–286.
- [11] O. D. KELLOGG, *Foundations of Potential Theory*, Dover Publications, New York, 1953.
- [12] N. KONDA AND F. ERDOGAN, *The mixed mode crack problem in a nonhomogeneous elastic medium*, *Engineering Fracture Mechanics*, 47 (1994), pp. 533–545.
- [13] B. Q. LI AND J. W. EVANS, *Boundary element solution of heat convection-diffusion problems*, *Journal of Computational Physics*, 93 (1991), pp. 255–272.
- [14] G. MAIER, M. DILIGENTI, AND A. CARINI, *A variational approach to boundary element elastodynamic analysis and extension to multidomain problems*, *Comp. Meth. Appl. Engng.*, 92 (1991), pp. 193–213.
- [15] A. J. MARKWORTH, K. S. RAMESH, AND W. P. P. JR., *Modelling studies applied to functionally graded materials*, *Journal of Materials Science*, 30 (1995), pp. 2183–2193.
- [16] F. W. J. OLVER, *Bessel functions of integer order*, in *Handbook of mathematical functions*, M. Abramowitz and I. E. Stegun, eds., National Bureau of Standards, Washington, D.C., 1972, ch. 9, pp. 355–434.
- [17] H. POWER, *On the existence of Kassab and Divo’s generalized boundary integral equation formulation for isotropic heterogeneous steady state heat conduction problems*, *Engrg. Analy. Boundary Elements*, 20 (1997), pp. 341–345.
- [18] R. P. SHAW, *Green’s functions for heterogeneous media potential problems*, *Engrg. Analy. Boundary Elements*, 13 (1994), pp. 219–221.
- [19] R. P. SHAW AND N. MAKRIS, *Green’s functions for Helmholtz and Laplace equations in heterogeneous media*, *Engrg. Analy. Boundary Elements*, 10 (1992), pp. 179–183.

- [20] R. P. SHAW AND G. D. MANOLIS, *A generalized Helmholtz equation fundamental solution using a conformal mapping and dependent variable transformation*, *Engrg. Analy. Boundary Elements*, 24 (2000), pp. 177–188.
- [21] S. SIRTORI, *General stress analysis method by means of integral equations and boundary elements*, *Meccanica*, 14 (1979), pp. 210–218.
- [22] S. SIRTORI, G. MAIER, G. NOVATI, AND S. MICCOLI, *A Galerkin symmetric boundary element method in elasticity: formulation and implementation*, *Int. J. Numer. Meth. Engrg.*, 35 (1992), pp. 255–282.
- [23] S. SURESH AND A. MORTENSEN, *Fundamentals of Functionally Graded Materials*, The Institute of Materials, IOM Communications Ltd., London, 1998.
- [24] C. VRETTOS, *Surface Green's functions for continuously nonhomogeneous soil*, in *Computer Methods and Advances in Geomechanics*, Beer, Booker, and Carter, eds., Rotterdam, 1991, Balkema, pp. 801–804.
- [25] L. C. WROBEL. Personal communication.

Appendix A: Symmetric Kernels

The Symmetric-Galerkin method [8, 14, 21, 22] is a highly effective numerical technique for boundary integral analysis. As the name implies, it utilizes the Galerkin approximation to induce a symmetric coefficient matrix. The symmetry comes about because of the symmetry properties of the kernel functions in the integral equations for surface temperature and for surface flux. Note that for the homogeneous Laplace equation, the fundamental solution is symmetric, $G(P, Q) = G(Q, P)$, but the FGM Green's function, Eq. (20), is not. Thus it would appear that a symmetric-Galerkin approximation is not possible.

In this section, the FGM boundary integral equations are re-formulated to allow a symmetric numerical implementation. In addition, formulas for all

of the required FGM kernel functions for $k(z)$ real,

$$k(z) = k_0 e^{2\beta_0 z} , \quad (39)$$

are conveniently summarized.

To obtain a symmetric matrix, the equations have to be written in terms of the surface flux,

$$\mathcal{F}(Q) = -k(z_Q) \frac{\partial}{\partial n} \phi(Q) \quad (40)$$

rather than the normal derivative. The equation for surface temperature $\phi(P)$ is therefore

$$\phi(P) + \int_{\Sigma} F(P, Q) \phi(Q) dQ = \int_{\Sigma} G_S(P, Q) \mathcal{F}(Q) dQ , \quad (41)$$

and in three dimensions the kernel functions are

$$\begin{aligned} G_S(P, Q) &= -\frac{G(P, Q)}{k(z_Q)} = -\frac{1}{4k_0\pi} \frac{e^{\beta_0(r-z_Q-z_P)}}{r} \\ F(P, Q) &= \frac{\partial}{\partial n} G(P, Q) - 2\beta_0 n_z G(P, Q) \\ &= -\frac{e^{\beta_0(r+R_z)}}{4\pi} \left(\frac{n \cdot R}{r^3} - \beta_0 \frac{n \cdot R}{r^2} + \beta_0 \frac{n_z}{r} \right) . \end{aligned} \quad (42)$$

Most importantly, note that $G_S(P, Q)$, unlike G , is symmetric with respect to P and Q . This is the first of three conditions needed for symmetry. The other two conditions involve the flux equation. Differentiating Eq. (41) with respect to P , dotting with $N = N(P)$, and multiplying by $-k(z_P)$ yields the corresponding equation for surface flux

$$\mathcal{F}(P) + \int_{\Sigma} W(P, Q) \phi(Q) dQ = \int_{\Sigma} S(P, Q) \mathcal{F}(Q) dQ . \quad (43)$$

The kernel functions, again for three dimensions, are computed to be

$$\begin{aligned} S(P, Q) &= -k(z_P) \frac{\partial}{\partial N} G_S(P, Q) \\ &= -\frac{e^{\beta_0(r-R_z)}}{4\pi} \left(-\frac{N \cdot R}{r^3} + \beta_0 \frac{N \cdot R}{r^2} + \beta_0 \frac{N_z}{r} \right) . \end{aligned} \quad (44)$$

and

$$\begin{aligned}
W(P, Q) &= -k(z_P) \frac{\partial}{\partial N} F(P, Q) \\
&= \frac{k_0}{4\pi} e^{\beta_0(r+z_Q+z_P)} \left(3 \frac{(n \cdot R)(N \cdot R)}{r^5} - 3\beta_0 \frac{(n \cdot R)(N \cdot R)}{r^4} \right. \\
&\quad + \frac{\beta_0^2 (n \cdot R)(N \cdot R) - \beta_0 (N_z n - n_z N) \cdot R - n \cdot N}{r^3} \\
&\quad \left. + \beta_0 \frac{\beta_0 (N_z n - n_z N) \cdot R + n \cdot N}{r^2} - \beta_0^2 \frac{N_z n_z}{r} \right) . \tag{45}
\end{aligned}$$

The additional symmetry requirements are that W must be symmetric, $W(P, Q) = W(Q, P)$, and that $S(P, Q) = F(Q, P)$. Interchanging Q and P implies replacing $N(P)$ with $n(Q)$ and changes the sign of R , and thus both conditions are seen to hold.

Two Dimensions

The two-dimensional kernel functions will involve the first kind Hankel functions

$$H_\nu^{(1)}(z) = J_\nu(z) + iY_\nu(z) , \tag{46}$$

where J_ν and Y_ν are the first and second kind Bessel functions of order ν [16]. To simplify notation, we drop the superscript (1), and in deriving the form of the kernels we make use of the derivative formulas

$$\frac{d}{dz} H_\nu(z) = -H_{\nu+1}(z) + \frac{\nu}{z} H_\nu(z) . \tag{47}$$

This formula also holds for the Bessel functions. Since the logarithmic singularity in $g(P, Q)$ is contained in the imaginary part Y_0 , it is not surprising that for $k(z)$ real, the Green's functions can be written in terms of this second kind Bessel function. Thus, for the potential equation,

$$\begin{aligned}
g_S(P, Q) &= \frac{1}{4k_0} e^{-\beta_0(z+z_P)} \Re\{Y_0(i\beta_0 r)\} \\
f(P, Q) &= \frac{\partial}{\partial n} g(P, Q) - 2\beta_0 n_z g(P, Q) \\
&= \frac{\beta_0}{4} e^{\beta_0 R_z} \left[-\Im\{Y_1(i\beta_0 r)\} \frac{n \cdot R}{r} + n_z \Re\{Y_0(i\beta_0 r)\} \right] , \tag{48}
\end{aligned}$$

where \Re and \Im denote the real and imaginary parts, respectively. The absence of the first kind Bessel functions stems from the fact that $J_0(i\beta_0 r)$ is real and $J_1(i\beta_0 r)$ is purely imaginary. This in turn following from the power series expansions for J_ν [16]. The corresponding kernels for the flux equation are

$$\begin{aligned}
s(P, Q) &= \frac{\beta_0}{4} e^{-\beta_0 R z} \left[\Im\{Y_1(i\beta_0 r)\} \frac{N \cdot R}{r} + N_z \Re\{Y_0(i\beta_0 r)\} \right] . \\
w(P, Q) &= -\frac{k_0 \beta_0}{4} e^{\beta_0(z+z_P)} \left(-\Re\{Y_2(i\beta_0 r)\} \frac{(n \cdot R)(N \cdot R)}{r^2} \right. \\
&\quad + \Im\{Y_1(i\beta_0 r)\} \left(\frac{n \cdot N}{r} - \beta_0 n_z \frac{N_z \cdot R}{r} + \beta_0 N_z \frac{n_z \cdot R}{r} \right) \\
&\quad \left. - \Re\{Y_0(i\beta_0 r)\} \beta_0 N_z n_z \right) .
\end{aligned} \tag{49}$$

Appendix B: 2D Green's Function Verification

```

##
## check 2D Green's function for the FGM Laplace equation
## k = exp(-2*I*a*z)
##
rsq := (x-xp)**2 + (z-zp)**2;
r := sqrt(rsq);
##
##
G := exp(-I*a*(z-zp))*H0(a*r);
Gxx := diff(G,x,x);
Gzz := diff(G,z,z);
Gz := diff(G,z);
##
LapG := Gxx + Gzz;
LapH := diff(H0(a*r),x,x) + diff(H0(a*r),z,z);
RM := expand(LapG - exp(-I*a*(z-zp))*LapH);
##
## LapG = RM + exp(-I*a*(z-zp))*LapH

```

```

## LapH = -a*a*H0(a*r) (Helmholtz equation) ==>
##
      LapG := RM - exp(-I*a*(z-zp))*a*a*H0(a*r);
##
## DE = Gxx + Gzz + 2*I*a*Gz = LapG + 2*I*a*Gz
##
      DE := LapG + 2*I*a*Gz;
      DE := expand(DE);

```

The end result, as expected, is that $DE = 0$.

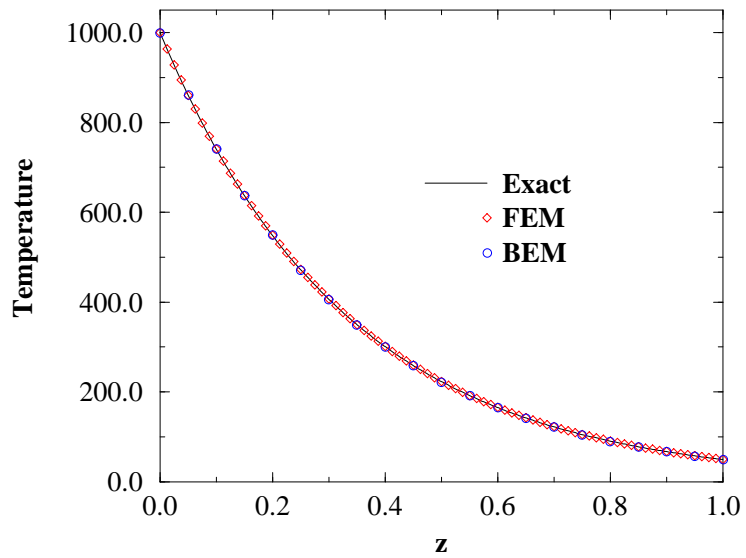


Figure 4: Temperature distribution in the FGM unit cube along the edge $[x = 1, y = 1]$.

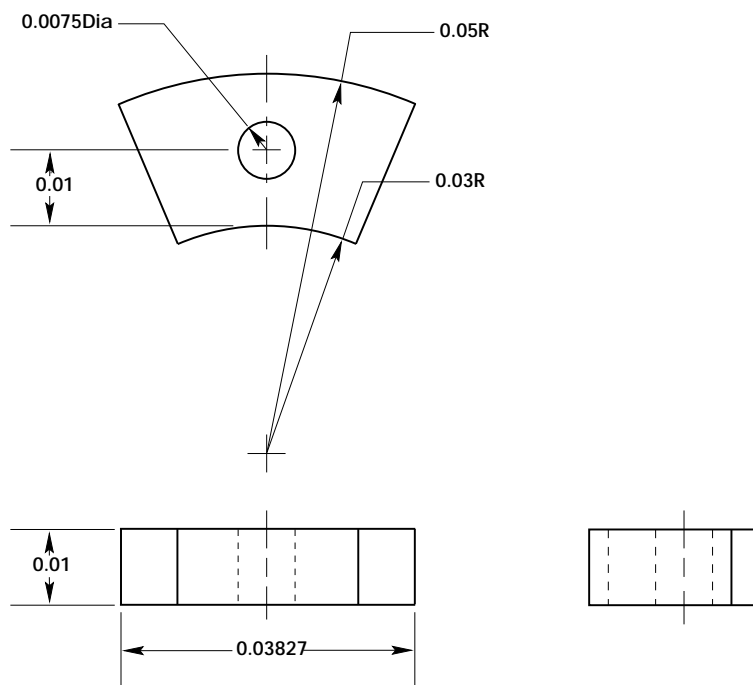


Figure 5: Geometry of the functionally graded rotor.

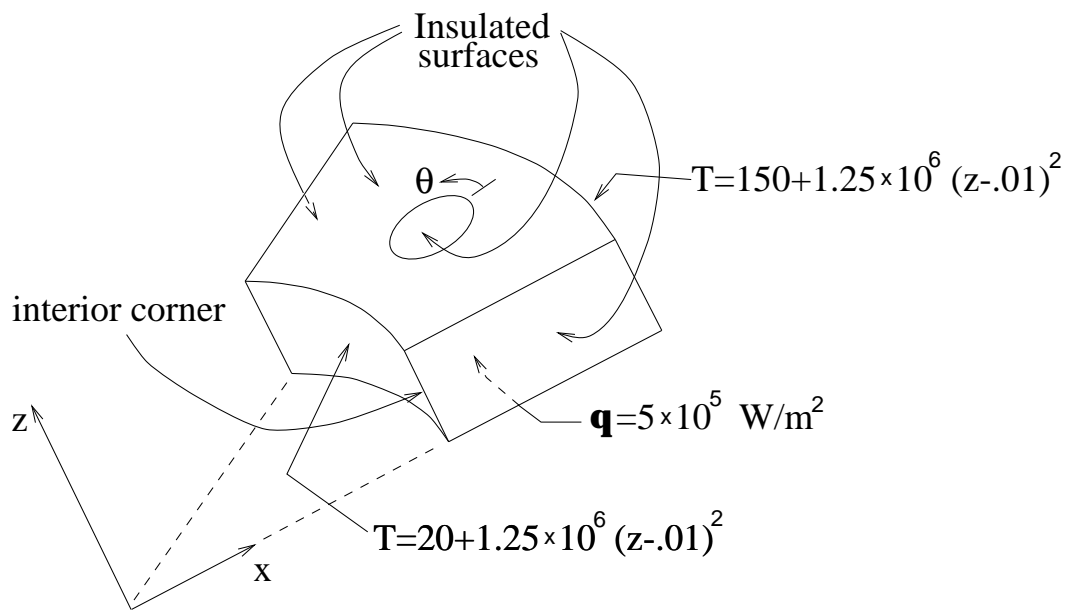


Figure 6: Thermal boundary conditions on the rotor.

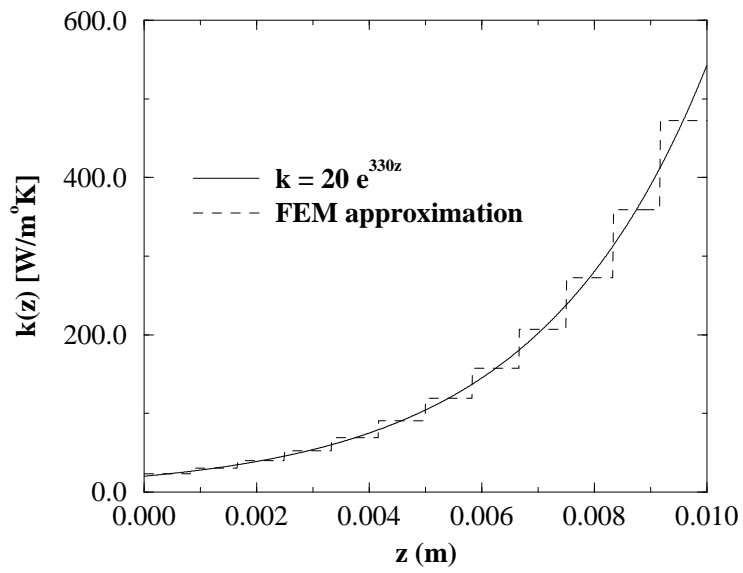


Figure 7: Thermal conductivity profiles for the computational models.

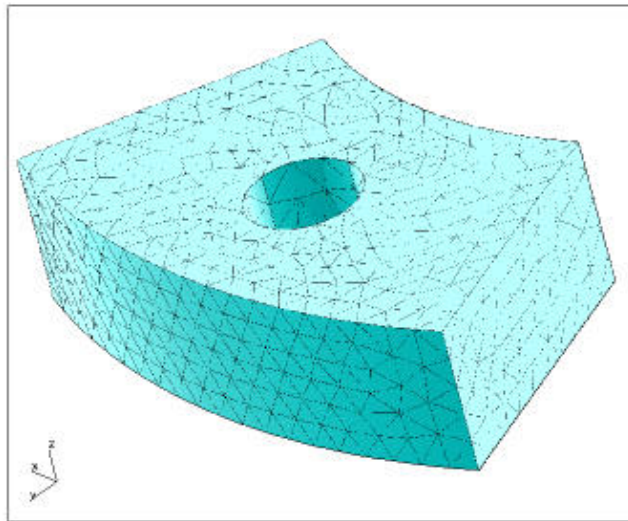


Figure 8: Surface mesh employed on the functionally graded rotor.

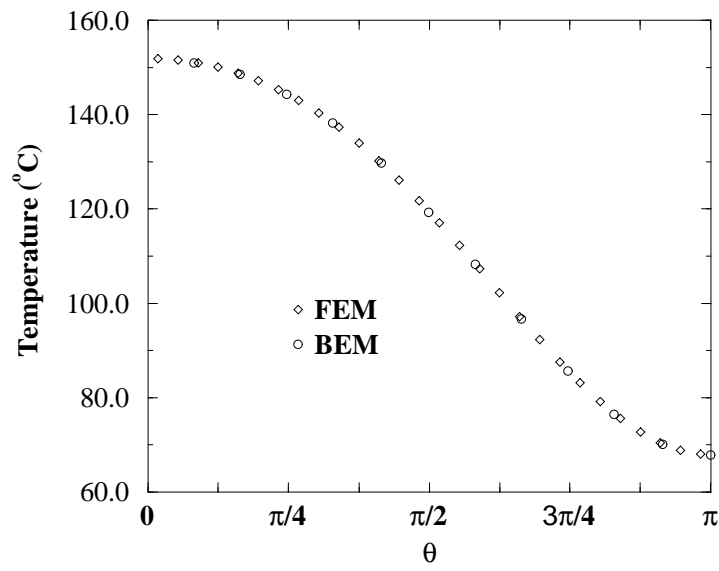


Figure 9: Temperature distribution around the hole on the $z = 0.01$ surface.

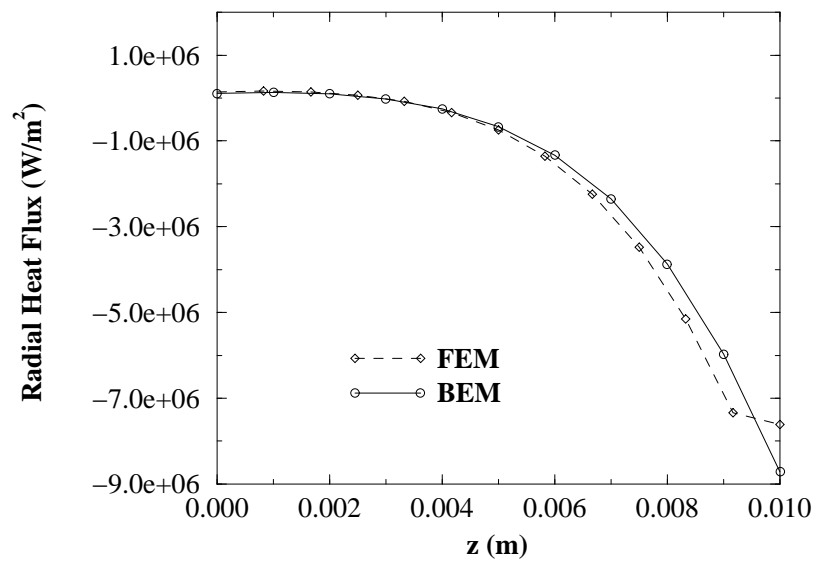


Figure 10: Radial heat flux along the inside corner.